194 *Biochemistry* **2011,** *50,* 194–206
DOI: 10.1021/bi101232y

BIOCHEMISTRY
including biophysical chemistry & molecular biology
Article

Characterization of an NADH-Dependent Persulfide Reductase from *Shewanella loihica* PV-4: Implications for the Mechanism of Sulfur Respiration via FAD-Dependent Enzymes[†,‡]

Megan D. Warner,[§] Vinita Lukose,[§] Kyu Hyun Lee,[§] Karlo Lopez,[∥] Matthew H. Sazinsky,[§] and Edward J. Crane III*[,§]

[§]*Pomona College Department of Chemistry, 645 North College Avenue, Claremont, California 91711, United States, and* [∥]*University of Central Missouri, Department of Biochemistry, Chemistry & Physics, W.C. Morris Building, Warrensburg, Missouri 64093, United States*

Received August 3, 2010; Revised Manuscript Received November 22, 2010

ABSTRACT: The NADH-dependent persulfide reductase (Npsr), a recently discovered member of the PNDOR family of flavoproteins that contains both the canonical flavoprotein reductase domain and a rhodanese domain, is proposed to be involved in the dissimilatory reduction of S^0 for *Shewanella loihica* PV-4. We have previously shown that polysulfide is a substrate for this enzyme, and a recently determined structure of a closely related enzyme (CoADR-Rhod from *Bacillus anthracis*) suggested the importance of a bound coenzyme A in the mechanism. The work described here shows that the *in vivo* oxidizing substrates of Npsr are the persulfides of small thiols such as CoA and glutathione. C43S, C531S, and C43,531S mutants were created to determine the role of the flavoprotein domain cysteine (C43) and the rhodanese domain cysteine (C531) in the mechanism. The absolute requirement for C43 in persulfide or DTNB reductase activity shows that this residue is involved in S−S bond breakage. C531 contributes to, but is not required for, catalysis of DTNB reduction, while it is absolutely required for reduction of any persulfide substrates. Titrations of the enzyme with NADH, dithionite, titanium(III), or TCEP demonstrate the presence of a mixed-disulfide between C43 and a tightly bound CoA, and structures of the C43 and C43,531S mutants confirm that this coenzyme A remains tightly bound to the enzyme in the absence of a C43−CoA S−S bond. The structure of Npsr suggests a likely site for binding and reaction with the persulfide substrate on the rhodanese domain. On the basis of kinetic, titration, and structural data, a mechanism for the reduction of persulfides by Npsr is proposed.

Respiration is often thought of solely as the creation of a proton motive force through the reduction of oxygen to water via the electron transport chain (aerobic respiration). While the term "anaerobic respiration" may sound like an oxymoron, a range of respiratory substrates other than oxygen are used by prokaryotes in reactions that have a significant impact on the cycling of many elements, influencing the geochemical makeup of the earth's surface and atmosphere (*1*−*3*). The ability of sulfur to interconvert through a range of oxidation states between 6+ to 2− has allowed bacteria and archaea to use sulfur and sulfur-containing compounds as substrates in both reductive and oxidative energy-conserving reactions, depending on the environment. The use of sulfur as an electron acceptor appears to have developed very early in the evolution of life, and while there is controversy regarding the identity of the first respiratory substrate (assuming there was only one "first" respiratory substrate), it is well accepted that sulfur reduction played an important role in the biochemistry of the early earth (*4*, *5*).

Dissimilatory sulfur respiration is the process by which sulfur, often in the form of polysulfide, is reduced to hydrogen sulfide ($S_n^{2-} + 2e^- + 2H^+ \rightarrow H_2S + S_{n-1}^{2-}$) (*6*), although the actual reaction is likely more complex as many forms of sulfur exist in the environment. Organisms in which sulfur respiration is observed often utilize a wide variety of sulfur derivatives as final electron acceptors, such as various allotropes of elemental sulfur, various sulfur salts, thiosulfates, thionates, DMSO, and di- and polysulfides. The most well characterized enzyme system involved in sulfur and thiosulfate reduction is the periplasmic membrane-bound polysulfide reductase complex (PsrABC), a three protein system comprised of a quinone-containing membrane anchor, an Fe−S-containing transfer protein, and an Fe−S/molybdopterin-containing subunit on which sulfur/polysulfide reduction occurs (*6*, *7*). In *Wolinella*, polysulfide has been shown to be delivered to this complex by the periplasmic Sud (sulfide dehydrogenase) protein, a member of the rhodanese class of proteins (*8*−*11*).

Shewanella oneidensis MR-1 was one of the first aerobic organisms found to be capable of dissimilatory reduction of sulfur while growing under anaerobic conditions, and with the exception of *S. denitrificans*, the ability to use sulfur as a final electron acceptor during growth on lactate or hydrogen appears to be a general characteristic of this genus (*12*−*14*). In an effort to understand the enzymology of sulfur reduction by *Shewanella* a survey of the currently sequenced *Shewanella* genomes was performed. It was found that all members of the genus, with the exception of *S. denitrificans*, contain a gene cluster homologous to the cluster in *W. succinogenes* that produces the PsrABC complex. Two of the species, *S. loihica* strain PV-4 and

[†]This work supported by the American Chemical Society Petroleum Research Fund Grant 46449-B4.

[‡]The coordinates and structure factors for wild-type, C531S, and C43,531S *Shewanella loihica* PV-4 NPSR have been deposited in the Protein Data Bank as entries 3NTA, 3NTD, and 3NT6, respectively.

*Corresponding author. Edward J. Crane, III, Pomona College Department of Chemistry, 645 North College Avenue, Claremont, CA 91711. Phone: (909) 607-9634. Fax: (909) 607-7726. E-mail: ej.crane@pomona.edu.

 Published on Web 11/23/2010

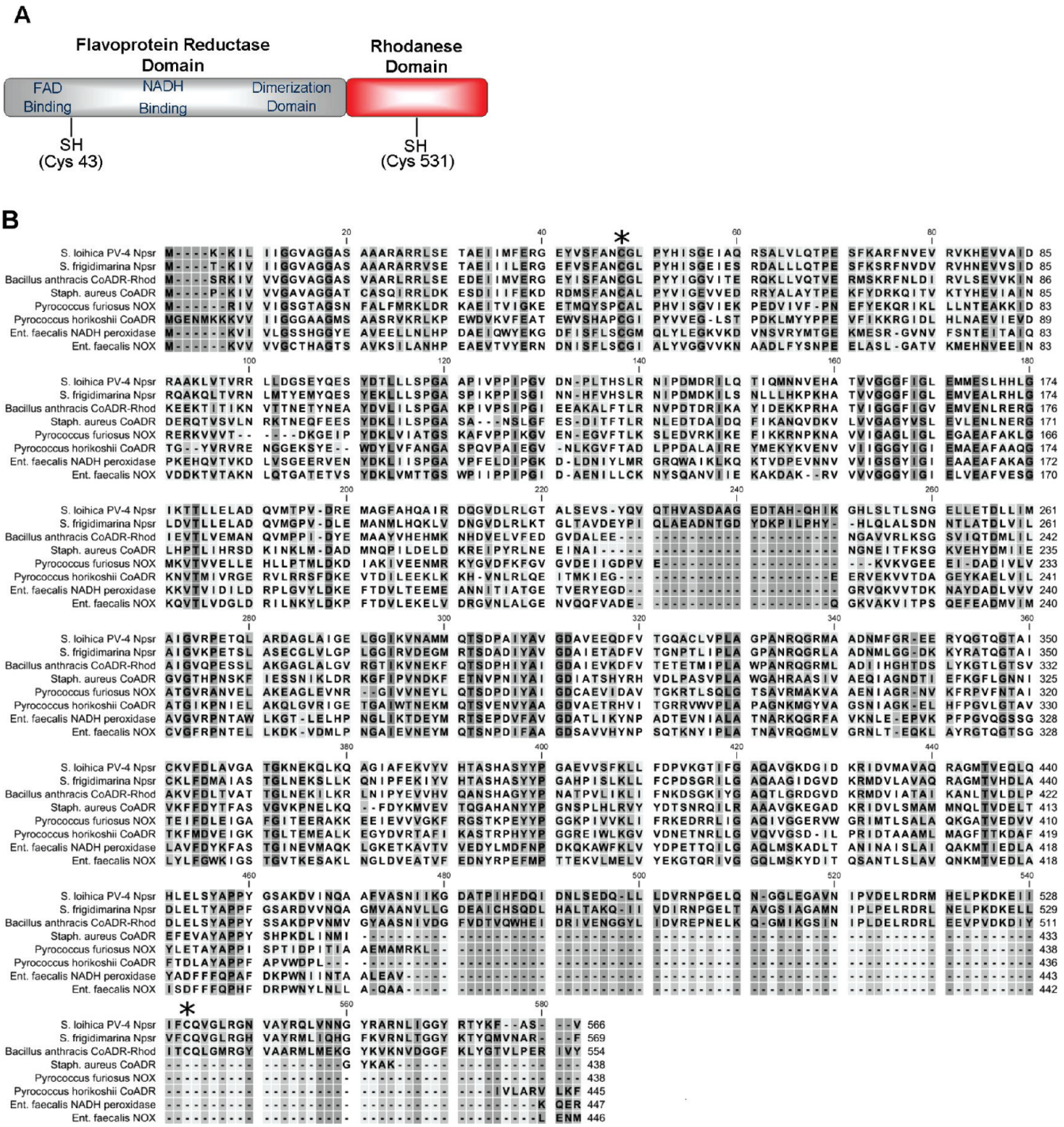

FIGURE 1: (A) Cartoon representation of the primary structure of the Npsr showing the two conserved cysteines. (B) Multiple sequence alignment of single-cysteine containing members of the PNDOR class of enzymes. The "single-cysteine" refers to the single active-site cysteine that corresponds to Cys 43 of the Npsr protein, the cysteines corresponding to C43 and C531 are marked with "∗". The alignment was performed with CLUSTAL W. The GenBank accession numbers for the enzymes are as follows: *S. loihica* PV-4 Npsr (YP_001092860), *S. frigidamarina* putative Npsr (EAN75345), *Bacillus anthracis* CoADR-Rhod (NP_843296.1). *Staphylococcus aureus* CoADR (AF041467), *E. faecalis* NPX (P37062), *E. faecalis* NOX (P37061), *P. horikoshii* CoADR (O58308), *P. furiosus* NOX (PF_1430634).

S. frigidamarina, contain genes coding for a flavoprotein homologous to a coenzyme A-disulfide reductase from *Staphylococcus aureus* (*15*−*17*) and to the recently characterized Coenzyme A and NADH-dependent sulfur reductases from *Pyrococcus horikoshii* and *furiosus* (*18*, *19*).

The N-terminus of the *Shewanella* homologue shows extensive conservation in the substrate and coenzyme binding regions and in the catalytic center when compared to members of the pyridine nucleotide-dependent oxidoreductase (PNDOR) family (Figure 1A (*20*)). However, it also contains an ∼100 amino acid C-terminal domain homologous to the rhodaneses, small (32 kDa or less) proteins characterized by their ability to catalyze the transfer of a sulfane sulfur to an acceptor via a double-displacement mechanism with a persulfide intermediate (*21*−*27*). The C-terminal domain is also homologous to the small polysulfide carrier protein Sud from *Wolinella* (Figure 1A (*8*, *9*, *28*−*30*)) and includes an absolutely conserved cysteine that acts as the polysulfide carrier on the Sud protein (Figure 1A,B).

Table 1: Primers for Isolation and Mutation of Npsr

Genomic Isolation	
forward	5′-GACGACGACAAGATGAAGAAGATACTGATTATTGGTGG-3′
reverse	5′-GAGGAGGAAGCCCGGTTTACACGCTGGCGAACTTG-3′
C43S Mutation	
forward	5′-CCTTTGCCAACTCTGGCCTGCCTTATC-3′
reverse	5′-GATAAGGCAGGCCAGAGTTGGCAAAGG-3′
C531S Mutation	
forward	5′-GGAGATCATCATCTTCTCTCAGGTGGGTCTGCGGGGC-3′
reverse	5′-GCCCCGCAGACCCACCTGAGAGAAGATGATGATCTCC-3′

Homologues to this approximately 570 amino acid flavoprotein/rhodanese fusion protein are also contained in a diverse range of other microbial genomes, including pathogens such as the γ-proteobacterium *Cholera vibrio*, *Bacillus anthracis*, *Clostridium perfringens*, and *Clostridium botulinum*.

Previous studies in this laboratory have shown that this flavoprotein/rhodanese fusion protein is capable of catalyzing the reduction of polysulfide by NADH (*31*), and the crystal structure of a homologue from *Bacillus anthracis* was recently determined (*32*). In the studies described below, we have further characterized the mechanism of this enzyme, which we have named NADH-dependent persulfide reductase or Npsr,[1] from *Shewanella loihica* PV-4 using a combination of structural, steady-state kinetic and titration studies. This work demonstrates that the physiological oxidizing substrate for this enzyme is a persulfide, in the form of a coenzyme A, glutathione, or other thiol persulfide or polysulfide. The rhodanese "tail" cysteine is proposed to attack the persulfide sulfur, which is held in place by interactions with an obvious pocket adjacent to the Cys531 persulfide sulfur observed in the structure, which was solved to 2.0 Å resolution. The tightly bound coenzyme A thiol of Npsr fulfills the role played by the second active site cysteine present in the closely related glutathione reductase in our proposed mechanism, turning the apparently single-cysteine active site of Npsr into an active site more analogous to that of the two-cysteine active site of related PNDOR enzymes.

MATERIALS AND METHODS

Cloning of Npsr and Npsr Mutants. Wild-type Npsr was amplified from *S. loihica* genomic DNA using primers (Invitrogen) given in Table 1 and cloned into a pET-21b or pET-32 EK/LIC vector (Novagen) using standard recombinant DNA technologies. Both plasmids incorporate a His_6 affinity tag and carry ampicillin resistance. The pET-32 EK/LIC vector also contained a thioredoxin tag; however, protein from both vectors was found to have identical activity and so Npsr with and without the thioredoxin tag was used interchangeably in the experiments described below. The C43S, C531S, and C43,531S mutations were created using a site-directed mutagenesis kit (Quikchange, Stratagene).

Overexpression and Purification. Npsr was overexpressed in *Escherichia coli* BL21(DE3) (Invitrogen) in Terrific Broth (EMD) containing 100 μg/mL ampicillin and grown at 37 °C until an OD_{600} of ∼0.7−0.9, when IPTG (Research Products, Inc.) was added to a final concentration of 1 mM. Protein expression was allowed to continue for 14 h at 37 °C, and cells were harvested via centrifugation at 8 000*g* for 20 min. Cells were lysed via sonication in wash buffer (50 mM Tris, pH 7.4, 200 mM NaCl, 20 mM imidazole), centrifuged at 15 000*g* for 2 h to remove cell debris, and the crude extract was applied to a preconditioned Ni-NTA column via an AKTA-FPLC. The column was washed with 10 column volumes of wash buffer and eluted with 50 mM Tris, 200 mM NaCl, and 250 mM imidazole. The protein was further purified by size-exclusion chromatography on a 26 cm × 60 cm Sephacryl S-200 HR column in 50 mM Tris, pH 7.5. Purity was confirmed by SDS-PAGE and an absorbance spectrum. Purified protein was flash frozen in liquid N_2 and stored at −80 °C until further use. A typical purification yielded ∼20 mg of Npsr per liter of media. The specific activity of the wild-type protein, as measured by the NADH-dependent DTNB reductase activity, was determined to be 27.4 U mg^{-1}, with a unit equal to the amount of enzyme required to oxidize 1 μmol of NADH in 1 min at 100 μM NADH and 1 mM DTNB in 50 mM Tris, pH 7.5 at 23 °C.

DTNB Steady-State Assays and Determination of the Flavin Extinction Coefficient. Steady-state kinetic assays were carried out at 25 °C in 2 mM DTNB (5,5′-dithiobis-(2-nitrobenzoic acid) (Sigma), 170 μM NADH (Sigma), and 10−50 nM enzyme in 50 mM Tris buffer, pH 7.5. The concentration of DTNB or NADH was varied to obtain kinetic parameters for these substrates. TNB (2-nitro-5-thiobenzoate, ε_{412} = 13 600 M^{-1} cm^{-1}) formation was monitored on a Cary 50 U spectrophotometer equipped with a Peltier cell. Protein concentrations were determined using the Bio-Rad Protein Assay dye with bovine serum albumin (BSA) as a standard. The extinction coefficient of the enzyme-bound FAD was determined to be 11 390 M^{-1} cm^{-1} using a previously described method (*19*).

Polysulfide, Sulfur, and Persulfide Steady-State Assays. Polysulfide reductase experiments were performed anaerobically in 0.5 M Tris, pH 8.5 using previously described techniques to maintain anaerobic conditions (*19*, *31*). Polysulfide was added to the cuvette via a gastight Hamilton syringe with a threaded plunger to initiate the reaction, which was monitored by the disappearance of NADH at 340 nm (ε = 6220 M^{-1} cm^{-1}). Measurement of sulfide produced during S^0 reduction was performed using the methylene blue method described previously (*18*, *31*, *33*). Thiol-persulfide assays were performed in a manner similar to that of the DTNB kinetic assays. Thiol-persulfide substrate was formed via a protocol modified from Williamson et al. (*38*). Sodium sulfide (∼5 mM) was incubated aerobically in 1 M potassium phosphate, pH 7.5, at room temperature with oxidized thiol (oxidized coenzyme A, oxidized glutathione, or DTNB) at concentrations ranging from 7.5−120 μM for 15 min. High concentrations of phosphate buffer were necessary to ensure a neutral pH for the assay due to the high basicity of sodium sulfide, which is in excess during this experiment. Incubation was performed in a hood due to the release of small amounts of hydrogen sulfide gas upon reaction of excess Na_2S with air. Immediately following incubation, NADH (100 μM) and enzyme (34 nM) were added to the solution and

[1]Abbreviations: Npsr, NADH-dependent persulfide reductase; CoADR, coenzyme A disulfide reductase (EC No. 1.8.1.14); DTNB, 5,5-dithiobis(2-nitrobenzoic acid); TNB, 5-thiobis(2-nitrobenzoic acid; EH_2, two-electron reduced enzyme; EH_4, four-electron reduced enzyme; IPTG, isopropyl thio-β-D-galactoside; TCEP, tris-(2-carboxyethyl)phosphine; NOX, NADH oxidase.

Table 2: X-ray Data Collection and Refinement Statistics

	wildtype (SeMet)	C531S (native)	C43,531S (SeMet)
	Data Collection		
beamline	SSRL 12-2	SSRL 12-2	SSRL 12-2
wavelength (Å)	0.979	0.979	0.917
space group	*P*3	*P*3	*P*3
unit cell dimensions (Å)	134.3 × 134.3 × 81.2	133.7 × 133.7 × 79.7	133.7 × 133.7 × 79.2
resolution range (Å)	40.6−2.00	38.3−1.99	38.3−2.00
total reflections	1 121 617	462 266	1 154 564
unique reflections	108 110	109 330	107 016
completeness (%)[a]	99.5 (96.4)	99.8 (99.7)	99.8 (97.5)
$I/\sigma(I)$[a]	13.8 (4.5)	15.8 (6.9)	14.7 (4.9)
R_{sym} (%)[a,b]	8.6 (44.9)	9.2 (41.0)	8.0 (47.8)
	Refinement		
R_{cryst} (%)[c]	16.8	24.3	18.7
R_{free} (%)[d]	19.0	27.5	21.2
average *B*-value (Å^2)	23.4	18.8	20.8
r.m.s. deviation bond length (Å)	0.040	0.029	0.031
r.m.s. deviation bond angles (deg)	2.67	2.35	2.62
no. protein atoms	8602	8595	8600
no. nonprotein atoms	202	202	202
water molecules	571	608	547
PDB Code	3NTA	3NTD	3NT6

[a]Values in parentheses are for the highest resolution shell. [b]$R_{sym} = \Sigma_i\Sigma_{hkl}|I_i(hkl) - \langle I(hkl)\rangle|/\Sigma_{hk}\langle I(hkl)\rangle$, where $I_i(hkl)$ is the *i*th measured diffraction intensity and $\langle I(hkl)\rangle$ is the mean intensity for the Miller index (*hkl*). [c]$R_{cryst} = \Sigma_{hkl}||F_o(hkl)| - |F_c(hkl)||/\Sigma_{hkl}|F_o(hkl)|$. [d]$R_{free} = R_{cryst}$ for a test set of reflections (5% in each case).

enzyme turnover monitored by disappearance of NADH. Controls were run with thiol, disulfide, and Na_2S with and without enzyme or NADH present to ensure these compounds did not react with NADH or enzyme independently. The amounts of reagent and enzyme were scaled down proportionately when using DTNB as the oxidized thiol due to interference by the yellow TNB under concentrated conditions. Kinetic parameters (K_m and V_{max}) for enzymes with detectable rates were determined using a curve-fitting program (*34*).

Anaerobic Titrations. Enzyme was made anaerobic via gas vacuum cycling using nitrogen gas in custom-made anaerobic titrating cuvettes. NADH, NADPH, dithionite, TCEP, or titanium(III) were added as reducing agents via a custom-made anaerobic titrating syringe with a screw-controlled plunger. For dithionite and titanium titrations, benzyl viologen (final concentration, 0.5 μM) was added as a redox mediator. All titrations were performed with enzyme concentrations between 20 and 50 μM in 50 mM Tris, pH 7.4, except for titanium(III) titrations which required 1 M Tris, pH 7.4 to maintain pH. Titrations were monitored on a Cary 50 spectrophotometer equipped with a Peltier cell. NADH titrations were also monitored via fluorescence on a Peltier cell-equipped Cary Eclipse fluorometer.

Protein Crystallization. Wild-type and mutant enzymes were concentrated to 100 μM following exchange into 50 mM MOPS, pH 7.0, and 5% glycerol buffer and crystallized at room temperature (~20 °C) in hanging drop plates with 75−100 mM sodium acetate, pH 4.7, 50−100 mM ammonium acetate, 4−8% PEG 8000, and 0.01% sodium azide. Yellow crystals with dimensions of approximately 0.1 mm × 0.1 mm × 0.3 mm appeared within 2−5 days. Before data collection, the crystals were harvested and flash frozen with liquid nitrogen in a cryosolution comprising the mother liquor and 25% glycerol.

Data Collection, Structure Determination, and Refinement. The diffraction data were collected at SSRL on BL12-2. The crystals belonged to the space group *P*3 with unit dimensions $a = b = 133.4$ Å and $c = 79.5$ Å and contained two monomers per asymmetric unit. The reflections were indexed and scaled using HKL2000 (*35*). Each of the crystals had a significant pseudomerohedral twinning fraction, ranging from 25 to 45%. Molecular replacement was performed with Phaser (*36*) using a *Bacillus anthracis* Npsr homologue (*32*). The model was manually built in Coot (*37*) and refined using Refmac5 (*38*) in the CCP4 suite of programs (*39*). TLS parameters were applied to each refinement. All data processing and model refinement statistics are listed in Table 2. Structural analysis was performed by using PROCHECK (*40*) and indicated 96% and 4% of residues fell into preferred and allowed regions of a Ramachandran plot, respectively. Coordinates for wild-type, C531S, and C43,531S have been deposited in the Protein Data Bank.

RESULTS

Substrate Specificity and DTNB Reductase Activity. Npsr does not show any detectable NADH peroxidase activity and only a faint NADH oxidase activity and, most surprisingly, does not show any detectable NAD(P)H-dependent coenzyme A disulfide reductase activity despite similarities to enzymes with these abilities (Table 3). The enzyme does, however, exhibit NADH-dependent DTNB reductase activty that can be conveniently measured under aerobic conditions. At 25 °C the wild-type enzyme shows a k_{cat} of 30.0 s^{-1}, a $K_{m\ app}$ of 12.6 μM for NADH at saturating DTNB. and a $K_{m\ app}$ of 116 μM for DTNB in the presence of saturating NADH. No DTNB reductase or polysulfide reductase activity was detected with NADPH. Table 3 gives the kinetic parameters for the wild-type, C43S, C531S, and C43,531S mutant Npsr enzymes.

Mutation of the active site cysteine to a serine residue (C43S) gave no detectable rate of DTNB reduction regardless of the

Table 3: Kinetic Constants for Npsr, C43S, C531S, and C43,531S Npsr

activity	k_{cat} s^{-1}	K_m NADH μM	K_m ox. subs. μM	k_{cat}/K_m (ox. sub) M^{-1} s^{-1}
		Wild-Type (Recombinant)		
DTNB reductase, 25 °C[b]	30 ± 1.9	12.6 ± 2.1	116 ± 20	2.6×10^5
DTNB reductase, 5 °C	12 ± 0.8	n.d.[a]	124 ± 25	8.5×10^4
TNB persulfide reductase, 25 °C	144 ± 13.2	n.d.[a]	9.9 ± 2.6	1.5×10^7
CoA persulfide reductase 25 °C[c]	87 ± 17	n.d.[a]	54 ± 11	1.6×10^6
glutathione persulfide reductase, 25 °C	59.8 ± 3.8	n.d.[a]	39.8 ± 8.2	1.5×10^6
polysulfide reductase (1 mM CoA)[d]	28 ± 7.0	60 ± 15	n.d.[a]	
polysulfide reductase (no CoA)	23 ± 5.8	110 ± 28	n.d.[a]	
sulfur reductase (no CoA)[b]	0.004[e]	n.d.[a]	solid substrate	
		C43S Mutant		
DTNB reductase 25 °C	not detected			
CoA persulfide reductase 25 °C	not detected			
TNB persulfide reductase, 25 °C	not detected			
		C531S Mutant		
DTNB reductase, 25 °C	16 ± 2.0	n.d.[a]	574 ± 185	2.9×10^4
DTNB reductase, 5 °C	8.7 ± 0.5	n.d.[a]	540 ± 68	1.6×10^4
TNB persulfide reductase, 25 °C	not detected			
CoA persulfide reductase, 25 °C	not detected			
glutathione persulfide reductase, 25 °C	not detected			
		C43,531S mutant		
DTNB reductase	not detected			
polysulfide reductase	not detected			
CoA persulfide reductase 25 °C	not detected			

[a]n.d. indicates the activity was not determined. [b]DTNB reductase and sulfur reductase activity were determined in 50 mM Tris, pH 7.5. [c]Persulfide assay determined in 1 M phosphate buffer pH 7.5. [d]Polysulfide reductase activity was determined in 0.50 M Tris, 2 mM polysulfide, pH 8.50 under anaerobic conditions. [e]Calculated from observed rate at 14 mM NADH, 32.5 μM Npsr in the presence of solid S^0.

presence or absence of the rhodanese domain cysteine (C531), confirming the essential role of this residue in catalyzing the cleavage of any S−S bond with this enzyme. DTNB reductase activity is observed with Npsr in which the rhodanese domain cysteine residue has been replaced by serine (C531S), although a loss of catalytic efficiency is observed; the C531S mutant shows a 50% reduction in the k_{cat} and a 5-fold increase in the K_m for DTNB. This result suggests that while this residue contributes to the disulfide reductase activity it is not essential for this function.

Polysulfide Reductase Activity. Npsr also catalyzes an NADH-dependent polysulfide reductase activity (eq 1), as measured by NADH disappearance at 340 nm (*31*):

$$S_n^{2-} + NADH + H^+ \rightarrow S_{n-1}^{2-} + H_2S + NAD^+ \quad (1)$$

Extensive controls were conducted to ensure that the reaction being observed was in fact an enzyme-dependent polysulfide reduction; only small levels of background reactions were observed. As an example, when NADH and polysulfide were combined in the absence of enzyme, a small, nonlinear background rate was observed which was subtracted from the overall observed rate. No polysulfide reductase activity was observed with NADPH as the reducing substrate. The kinetic constants for the DTNB reductase activity and the polysulfide reductase activity are of similar orders of magnitude, with the $k_{cat}/K_{m\ NADH}$ for the DTNB reductase being roughly 5 times greater than that of the polysulfide reductase, due largely to the differences in $K_{m\ app}$ for NADH.

When the enzyme activity of the NADH-dependent reduction of solid sulfur by Npsr was determined, a remarkably slow rate was obtained (Table 3). In this assay the appearance of sulfide was measured over 10 h using a standard spectrophotometric assay for sulfide production (*33*). Attempts to recreate the NADH and coenzyme A-dependent sulfur reductase seen with the *P. furiosus* NADH-dependent sulfur reductase (*18*) were hampered by the interference of both reduced and oxidized coenzyme A with the standard methylene blue-forming assay used for detection of sulfide. While other research groups have not seen this interference and the method has been widely reported to be insensitive to thiols, in our hands we were not able to detect sulfide in the presence of oxidized or reduced coenzyme A, even in controls which were spiked with sodium sulfide. In the absence of coenzyme A, the assay worked as previously reported in the literature (*33*). The lower temperature of these assays, when compared to that of the pyroccocal enzyme, also meant that less of the insoluble S^0 substrate was in solution and available to the enzyme or for reaction with coenzyme A thiol, as the solubility of S^0 is highly temperature dependent (*41*).

Thiol-Persulfide Reductase Activity. Steady-state kinetic parameters for the coenzyme A persulfide substrate (CoA−S−SH + NADH → NAD^+ + CoA−SH + H^+) are shown in Table 3. Mutation of either or both C43 and C531 to serine resulted in the loss of detectable activity, showing that while C531 is not essential for breakage of the S−S bond with the DTNB substrate, it is essential for the persulfide reductase activity. Kinetic parameters show a 3-fold increase in k_{cat} and a slightly lower K_m with the CoA persulfide substrate compared to DTNB. The enzyme also shows a robust reductase activity with TNB and glutathione persulfides (R−S−S−H + NADH + H^+ → R−S−H + NAD^+ + H_2S). Likewise, these activities are absolutely

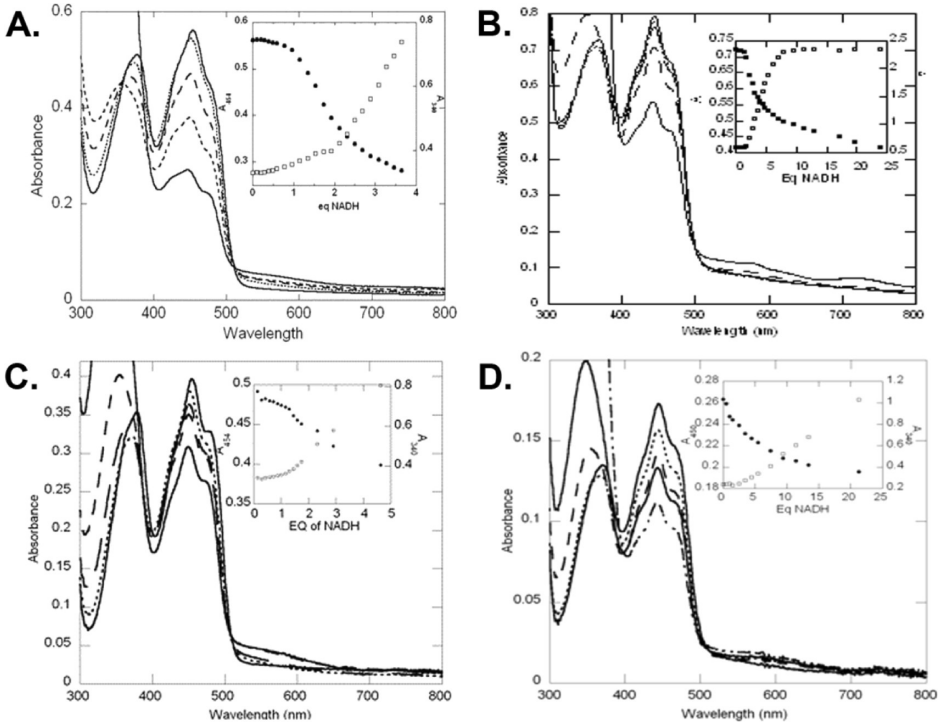

FIGURE 2: (A) Anaerobic reductive titration of wild-type Npsr with NADH monitored in a spectrophotometer. Spectra shown are at 0 (—), 1.0 (· · ·), 1.5 (– – –), 2.1 (- - -), and 6.9 (—) equiv of NADH. Inset: Plot of absorbance at 454 (●) and 340 (□) nm vs equivalents of NADH added. (B) Anaerobic reductive titration of C43S mutant Npsr with NADH monitored in a spectrophotometer. Spectra shown are at 0 (—), 1.3 (· · ·), 1.7 (– – –), 2.1 (- - -), and 6.8 (—) equiv of NADH. Inset: Plot of absorbance at 454 (●) and 340 (□) nm vs equivalents of NADH added. (C) Anaerobic reductive titration of C531S mutant Npsr with NADH monitored in a spectrophotometer . Spectra shown are at 0 (—), 1.0 (· · ·), 1.6 (– – –), 2.3 (- - -), and 4.6 (—) equiv of NADH. Inset: Plot of absorbance at 454 (●) and 340 (□) nm vs equivalents of NADH added. (D) Anaerobic reductive titration of C43,531S mutant Npsr with NADH monitored in a spectrophotometer. Spectra shown are at 0 (—), 1.0 (· · ·), 3.5 (– – –) 5.4 (—), and 13 (· · – – · ·) equiv of NADH. Inset: Plot of absorbance at 450 (●) and 340 (□) nm vs equivalents of NADH added.

dependent on the presence of both C43 and C531, suggesting a specific role for C531 in persulfide reduction.

Anaerobic trations of Npsr with NADH, Dithionite, and Titanium. When monitored via absorbance spectra, reduction of wild-type with NADH shows a blue shift of the 454 and 380 nm peaks from the bound FAD during addition of the first equivalent of NADH, although very little change is observed in the spectra, consistent with the reduction of an active site mixed disulfide enzyme (Figure 2A). These titrations were performed with enzyme as purified and without any addition of coenzyme A disulfide or polysulfide, which could further oxidize the enzyme. When greater than 1 equiv of NADH is added, reduction of the flavin occurs, although even with excess NADH, only half reduction of the dimer is ever achieved, indicating half-sites reactivity. These results are similar to those obtained by Wallen et al. (*32*), although the blue shift appears to be more pronounced and the degree of flavin reduction seems to be greater at 2 equiv of added NADH in the case of the *Shewanella* enzyme. *S. loihica* Npsr also shows remarkably strong fluorescence in the oxidized form (~300% that of free FAD, an unusual observation as in most flavoproteins FAD fluorescence is severely quenched, especially by aromatic and sulfur containing residues as well as disulfide bonds (*42*−*44*)) (Figure 3A). This fluorescence decreases greatly during reduction from the E to EH_2 form, providing a sensitive measure of the E → EH_2 conversion (Figure 3A). Reduction of the C531S mutant gave very similar results to that of the wild-type enzyme, including the blue-shift of the peaks attributed to FAD absorbance, and significant FAD fluorescence (Figures 2C and 3C). The C43,531S double mutant did not show this initial phase of reduction, and the bound FAD fluorescence falls to ~30% of free FAD (Figures 2D and 3D).

Reduction of the C43S mutant with NADH (Figures 2B and 3B) clearly shows different behavior from that of the wild-type enzyme, although like the wild-type enzyme there is some ambiguity regarding the equivalents of NADH required for the complete reaction to occur. The first phase of the titration seen with wild-type enzyme, where there is little increase at 340 nm during the addition of the first equivalent of NADH, is eliminated. This observation is consistent with the loss of a reducible nonflavin active center corresponding to Cys43. There is, however, a lag of approximately 1 equiv of NADH before the enzyme-bound FAD begins to reduce, as seen at 444 nm (Figure 3B, inset). The increase in absorbance at 340 nm, the slight decrease at 444 nm, and the development of broad absorbance at > 500 nm are consistent with this phase representing the binding of NADH to the C43S enzyme.

Reduction of wild-type enzyme with NADPH shows essentially similar results (data not shown), although the reaction is significantly slower, with each addition of NADPH requiring an equilibration time of hours compared to reduction by NADH, which occurs immediately upon addition of titrant. In addition, some precipitation of Npsr was observed over the long time period required for titrations with NADPH (24−48 h), making these experiments irreproducible. This result, when combined with the lack of any observed catalytic activity with NADPH, strongly suggests that Npsr has a definite preference for NADH over NADPH.

The addition of dithionite allowed for full reduction of the flavin to the EH_4 form of the enzyme, indicating that reduction of the first FAD results in a drop of the second FAD redox

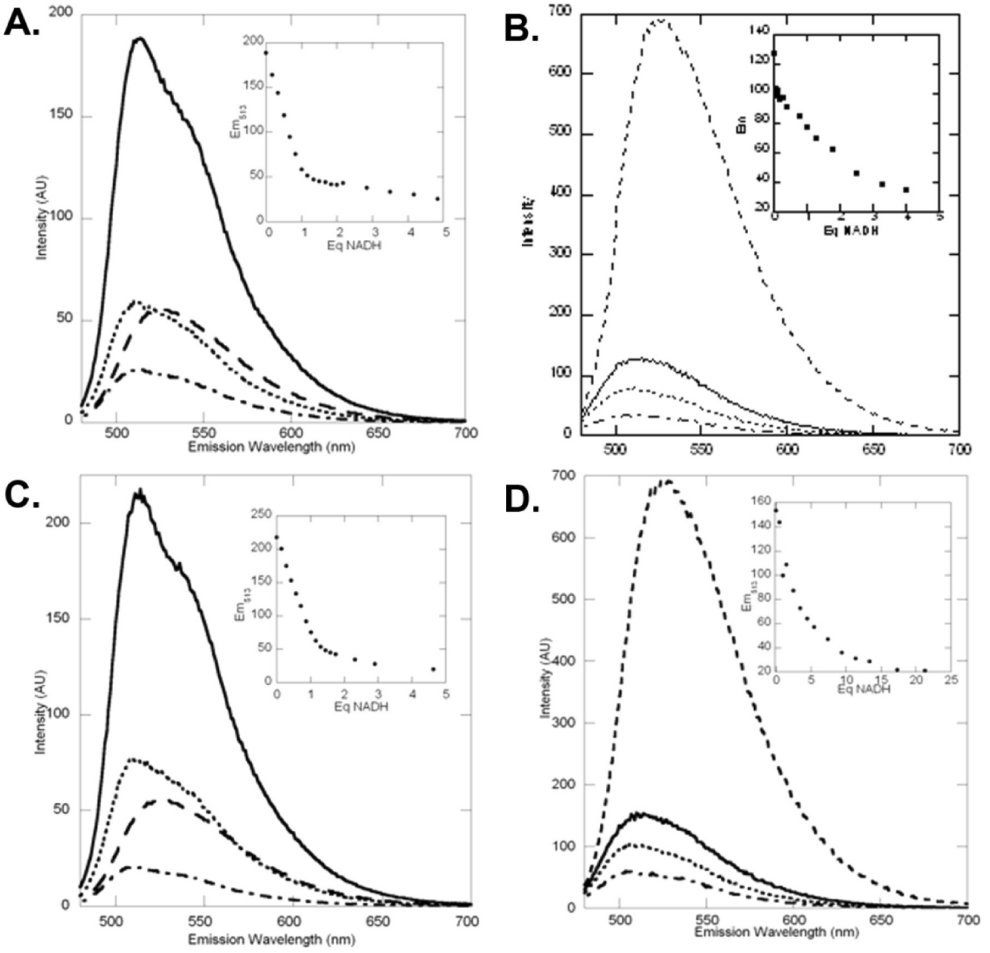

FIGURE 3: Anaerobic reductive titrations of (A) wildtype, (B) C43S, (C) C531S, and (D) C43,531S mutant Npsr with NADH as monitored by fluorescence where the excitation wavelength was 462 nm and the emission was monitored between 480 and 700 nm. Spectra shown are at 0 (—), 1.0 (· · ·) and 4.8 (— · — · —) equiv of NADH (- - -) along with free of FAD (— — —) of similar concentration. Inset: Plot of emission at 513 (●) nm vs equivalents of NADH added.

potentials to somewhere between −320 and −420 mV, although the process is extremely slow (data not shown). Reduction of the C43S mutant was never observed with dithionite, although this may represent a change in the kinetic rather than thermodynamic barrier for reduction of this mutant.

Since reduction of the enzyme with dithionite is extremely slow, taking days even in the presence of viologen mediator, and full reduction of the C43S mutant was never observed, the enzyme was titrated anaerobically with Ti(III). Relatively rapid full reduction of the flavin was observed during titration of the wild-type and enzyme with this reductant. This result also provides a narrower likely reduction potential for the second FAD during the $EH_2 \rightarrow EH_4$ reduction, as the reduction potential of Ti(III) → Ti(II) is −369 mV, placing the potential of the second FAD between −320 and −369 mV. This reducing agent has not yet been employed on any mutant enzyme.

Reduction of Npsr with TCEP. To probe the nature of the species which the first equivalent of NADH reduces, titrations were performed with TCEP (tris-(2-carboxyethyl)phosphine), a compound which selectively reduces disulfide bonds (Scheme 1 (*45*)). The absorbance spectrum of wild-type Npsr showed a blue shift identical to that observed during reduction with dithionite or NADH upon reduction with TCEP, consistent with the breakage of a S−S bond during the $E \rightarrow EH_2$ reduction.

Scheme 1

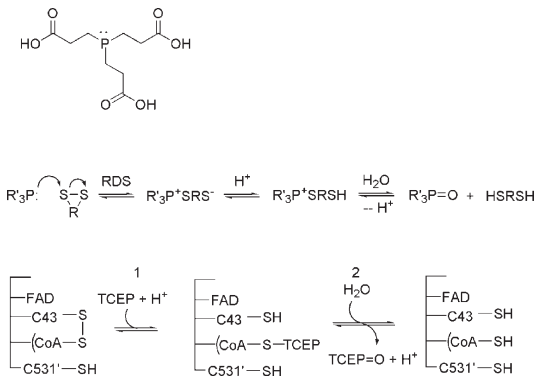

Crystal Structure of Wild-Type and Mutant Npsr. The structure of Npsr was solved to 2.0 Å resolution (Figure 4A). The folds of the wild-type and mutant enzymes are identical. Npsr exists as a homodimer with a 2-fold symmetry axis where each subunit contributes to the formation of the active site in the adjacent subunit. Individual subunits are comprised of two separate domains. The larger of these domains (residues 1−470) shows considerable similarity to CoADR from *S. aureus* and *B. anthracis*, while the other smaller domain (residues 471−566) shows similarity to structures from the rhodanese superfamily. Alignment of Npsr with the *B. anthracis* structure using Pymol

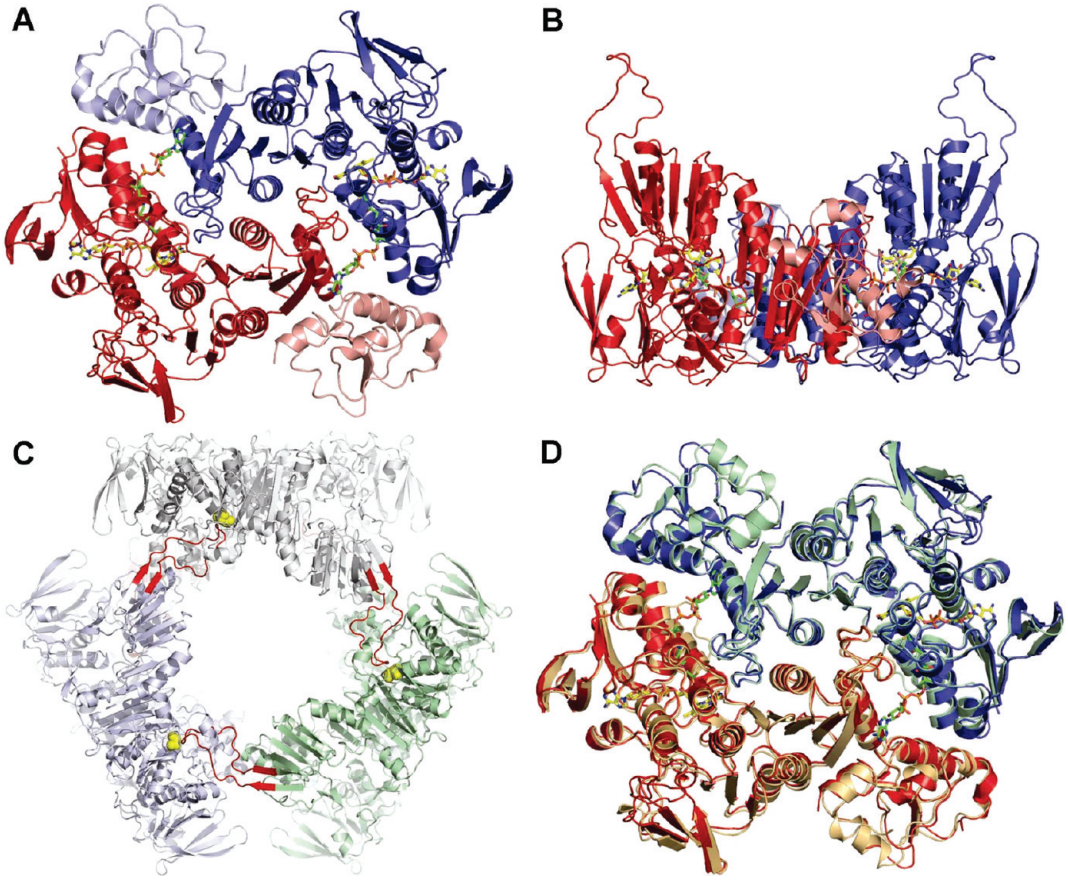

FIGURE 4: Structure of *Shewanella loihica* Npsr. (A) Ribbon structure of Npsr. The α and *β* subunits are depicted as blue and red helices, respectively. The rhodanese domains are shaded in a lighter version of the same color. Coenzyme A (green) and FAD (yellow) are depicted as sticks. (B) Rotation of Npsr by 90° depicting the loop comprising residues 220−245. (C) Crystal packing of Npsr. The 220−245 loop (red) from one monomer packs against the rhodanese domain of a second molecule near Cys 531 (yellow spheres). (D) Structural alignment of SLNpsr (red and blue) with BACoADR-RHD (green and tan) (PDB entry 3ICR). The rms deviation is 0.92 Å.

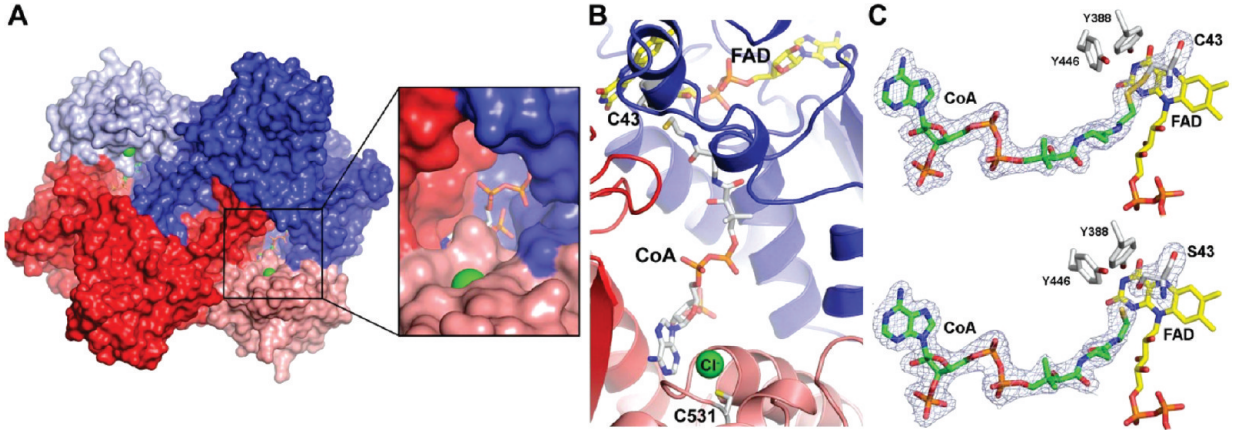

FIGURE 5: (A,B) Substrate access to the active site. All subunits and domains are colored as in Figure 4A, and in part A, the green sphere represents the location of C531 on the rhodanese domain. (C) Active site of (upper) wild-type CoaDRR and (lower) C43,531S CoaDRR. Simulated annealing 2Fo-Fc maps are depicted around the cofactors and C43 at 1*σ*.

shows a nearly identical fold, with an rmsd value of 0.92 Å^2 compared to all backbone atoms (Figure 4D). A point of difference between the structures is an additional loop (residues 225−245) on the *S. loihica* enzyme, which extends out from the main fold of the subunit (Figure 4B). These residues are not present in the homologues of enzymes that only contain a PNDOR domain, such as NADH peroxidase, NADH oxidase, and CoADR (Figure 1). Only a few Npsr homologues, such as those from *Vibrio cholera*, *Tolumonus auensis*, and *Shewanella frigidimarina*, contain this additional loop. The ordering of this region appears to be facilitated by the crystal packing (Figure 4C), whereby each loop interacts with a rhodanese domain on an adjacent dimer unit to aid the formation of the observed *P*3 symmetry.

Active Site. The walls of the active site are formed by the intersection of a flavoprotein domain of one subunit and the rhodanese and flavoprotein domain on the other subunit (shown as blue, pink, and red, respectively, in Figures 4A and 5A). A bound CoA molecule sits within this pocket on the flavoprotein

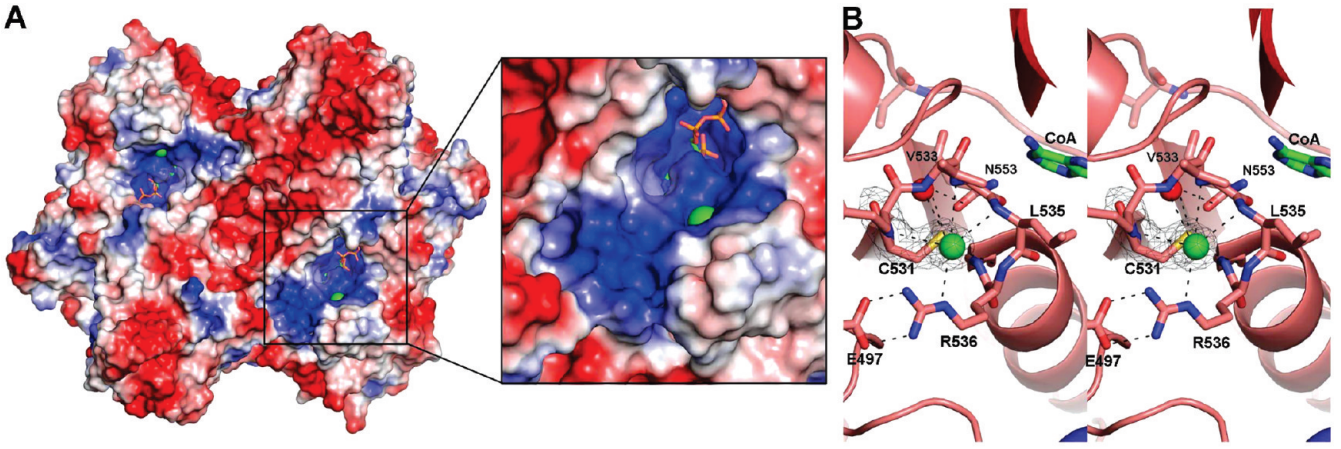

FIGURE 6: (A) Electrostatic surface map of SLNpsr. CoA is depicted as sticks and colored by atom type. The green sphere represents the location of C531 on the rhodanese domain. (B) Stereoview of chloride ion binding adjacent to C531 on the rhodanese domain. Chloride is depicted as a green sphere and is within 2.7−3.5 Å of several backbone amides. C531 sits 2.8 Å underneath the Cl^-, 3.0 Å above the R536 backbone amide, and H-bonds to a single water molecule, which is held in place by N553. The CoA adenine group (green) is also depicted.

subunit. Like other PNDOR enzymes, the CoA thiol lies adjacent to the active site cysteine (C43), two conserved tyrosines (Y388 and Y446), and the FAD isoalloxazine ring. In the oxidized form, C43 forms a mixed disulfide bond with CoA (Figure 5C, top). In the double mutant, electron density between S43 and CoA is absent, indicating CoA is not covalently bound in this structure but appears to be bound very tightly (Figure 5C, bottom). Examination of the Npsr and CoADR-RHD surfaces show a channel leading 23 Å from the buried active site CoA thiol to the surface exposed C531 on the rhodanese domain of the opposite subunit (Figure 5A,B). This path suggests how CoA may acquire substrate from C531 for reduction.

Rhodanese Domain. The rhodanese domain of one subunit is adjacent to the flavoprotein domain of the other and shows a fold consistent with members of the rhodanese superfamily. C531 nestles into a fairly electropositive groove on the rhodanase domain surface (Figure 6A). Located 2.9 Å above this cysteine in both subunits in the wild-type, C531S, and C43,531S proteins is a strong feature of spherical electron density that appears to correspond to a single atom (Figure 6B). Modeling this density as water resulted in residual difference density and an unreasonably low *B*-factor. Modeling the density as a chloride ion, however, which is present in the buffers, gives a more reasonable *B* value of ~30 $Å^2$ and accounts for all of the density in the region. This chlorine ion is held in place by an extensive network of potential hydrogen bond donors, which appear to create an ideal electropositive environment for holding a single negatively charged atom like sulfide in place (Figure 6B).

DISCUSSION

Summary of Differences between the S. loihica PV-4 Npsr and the B. anthracis CoADR-RHD. In addition to characterizing the reaction of Npsr with its physiological substrates (small thiol-peroxides), the kinetic and structural studies described here confirm many of the conclusions from the recently published structure of the homologous CoADR-RHD from *B. subtilis* (*32*), although there are significant differences. The main differences include (1) no loss of electron density was observed for the CoA pantatheine arm in the absence of a CoA−cysteine mixed disulfide bond in the case of the C43S Npsr mutants, indicating that the arm remains bound in position rather than becoming highly disordered, as seen with the synchrotron radiation induced reduction of the CoADR-RHD, (2) a distinct spherical region of electron density observed on the rhodanese domain of Npsr, attributed to a tightly bound chloride positioned in the proposed persulfide substrate binding site, which is not seen on the CoADR-RHD (although some indistinct density in a similar position is observed), (3) the presence of the loop between amino acids 221 and 241, which is only present on the *Shewanella* forms of the enzyme, and (4) the DTNB reductase activity of the Npsr C531 mutant is greater than that seen with the corresponding CoADR-RHD C514S mutant, an observation which may be due to experimental conditions. These differences are discussed in detail below.

Substrate Channeling. The X-ray and biochemical data provide greater insight into the mechanisms by which Npsr first acquires substrate and then reduces it. All Npsr and CoADR-RHD structures solved contain a coenzyme A molecule in the active site channel (*32*). Wallen et al. suggest this CoA acts as a transfer arm, first reacting with substrate on the C531 (*S. loihica*) residue and then transferring it to the active site cysteine (C43) for reduction (*32*). The basis for this proposed mechanism was the loss of electron density in the pantetheine arm upon reduction of the C43−CoA disulfide bond with synchrotron radiation. However, examination of the C43,531S double mutant crystal structure does not show disordering of the tightly bound CoA molecule. Despite the lack of either cysteine, the bound coenzyme A thiol lies 2.7 Å from the S43 −OH at the active site (Figure 5C). While this does not disprove the mechanism presented by Wallen et al., it does indicate that mere reduction or lack of an active site thiol at position 43 may not be enough to promote the arm mechanism to occur. A confounding factor in this analysis is the crystal packing, specifically the interaction of the rhodanese domain with of a loop (residues 225−245) from an adjacent Npsr molecule. This loop may be hindering interactions between CoA and the serine residue at position 531 (Figure 4B,C).

One mechanistic possibility to consider is that the rhodanese domain could alter its orientation throughout the catalytic cycle to facilitate either substrate binding and delivery to C531 or substrate transfer from C531 to the bound CoA thiol. An alignment of the *S. loihica* Npsr and *B. anthracis* structures shows very little deviation in both the folds and positioning of the different rhodanese and PNDOR domains. This similarity seems to suggest that the rhodanese domain itself likely does not move to accept a

Scheme 2

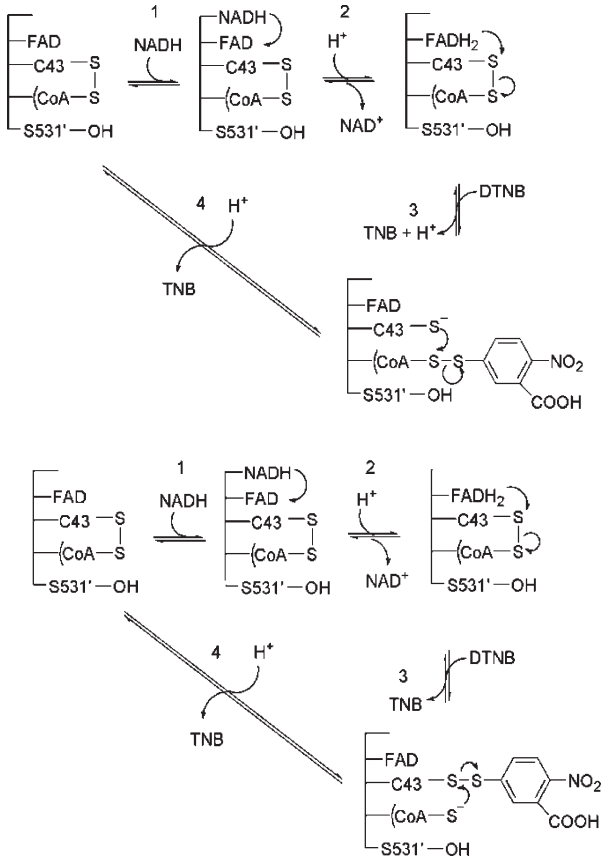

substrate, as some change in position of the domains would occur in crystal structures of different homologues if this were the case.

The structure of the rhodanese domain shows increased electron density near the 531 residue for all enzyme variations. This electron density has been modeled as a tightly bound chloride ion. Figure 6B shows the location of this chloride ion and the extensive network of potential hydrogen bond donors that create an electropositive environment necessary for holding this anion in place. Additional electron density near the rhodanese domain cysteine was also observed in one subunit of the *B. anthracis* enzyme but was not modeled because of its odd blobby shape. This observation allowed the authors to rule out the idea of a covalently linked persulfide in the structure (*32*).

The presence of the chloride ion in the Npsr structures may model how persulfide (S^{2-}) forms stable interactions with the conserved cysteine and the local peptide structure of the rhodanese domain. Such a mechanism is supported by evidence of a persulfide intermediate in rhodanese enzymes during sulfur transfer (*24*−*27*). This transfer occurs via a double-displacement mechanism whereby the active site cysteine interacts with a sulfane sulfur, forming a persulfide intermediate which then rapidly reacts with some sort of sulfur acceptor, transferring the sulfur to its target and regenerating the active site cysteine (Scheme 2) (*26*, *46*). The similarity of this region to the fold of rhodanese proteins along with the careful network positioning the chlorine atom suggests that such an intermediate could be at play for Npsr. Since such an intermediate would be short-lived, it is likely that the substrate would react to displace a neutral placeholder like a chlorine atom to initiate enzyme turnover. The electrostatic surface of the enzyme suggests how negatively charged thiol-persulfide substrates like CoA persulfide and glutathione persulfide are attracted to the electropositive surfaces near C531 of the rhodanese domain (Figure 6A) and make use of the extensive hydrogen-bonding network adjacent to the C531 residue to facilitate sulfide transfer.

Utilization of a cysteine-containing "acceptor site" near the surface of the protein and a cysteine-containing "reaction site" buried near the FAD appears to be a fairly common strategy for flavoprotein oxidoreductases, especially in the PNDOR class. One well-characterized example of this type of system is mercuric ion reductase, which uses one pair of surface-accessible cysteines in the removal of ligands from its Hg(II) substrate and a second pair at the active site to catalyze the reduction of Hg(II) (*47*, *48*). In another example, the mammalian selenoprotein thioredoxin reductase, the mechanism is somewhat more complex, with initial reduction of the thioredoxin substrate occurring via a C-terminal cysteine and selenocysteine, followed by reduction of the subsequent selenenylsulfide bond by the active site cysteine pair (*49*). Interestingly, in the case of the mammalian thioredoxin reductase, inactivation of the C-terminal selenocysteine results in enzyme that loses its activity with the physiological substrate thioredoxin but retains some activity with DTNB, very similar to the result seen with the Npsr C531S mutant, which has no activity toward its physiological persulfide substrates but retains significant activity with DTNB.

Steady State Kinetics. The wildtype enzyme shows a strong preference for persulfide substrates in steady-state kinetic assays, yielding k_{cat}s between 60 and 144 s^{-1}, compared to the ~30 s^{-1} values observed with DTNB and polysulfide. Because the coenzyme A and glutathione persulfide substrates appear to be stable for short periods under aerobic conditions, it is likely that in an anaerobic environment where both coenzyme A or other thiols and sulfide are present (such as within a cell), this compound could form. Evidence also suggests that CoA persulfide acts as a potential inhibitor of Acyl-CoA dehydrogenases in mammalian mitochondria (*50*, *51*). These observations, along with the excellent kinetic parameters achieved, suggest that thiol persulfides such as coenzyme A or glutathione persulfide are likely the *in vivo* substrates for this enzyme. The lack of catalytic turnover with any substrate upon mutation of cysteine 43 confirms it to be the active site residue, as observed in other homologous flavoenzymes (*15*, *17*−*19*, *32*, *52*).

The finding that the enzyme is relatively nonspecific with regard to the nature of the persulfide donor was initially surprising. However, the structure of the enzyme shows how such nonspecificity is possible. The main feature attracting the persulfide substrate to the enzyme seems to be the area of positive charge around C531, and no obvious specific binding site for the second substrate-level CoA is observed. The similarity of the k_{cat}/K_m values for all three persulfide substrates assayed and the nearly identical k_{cat}/K_m values for the more physiological CoA and glutathione persulfide substrates (Table 3) indicate that any thiol present in the cell could serve as a persulfide donor. The *S. loihica* genome contains the biosynthetic enzymes for glutathione and a glutathione reductase homologue, so it seems likely that both glutathione and CoA would be physiologically relevant persulfide donors to Npsr.

The differences in the activity of the rhodanese domain cysteine mutant (C531S) with different substrates suggest the DTNB reductase activity can operate by a different mechanism than the coenzyme A persulfide reductase activity. Residue C531 is essential for the mechanism by which any thiol-persulfide is reduced, while it is not for DTNB reduction. This differs

Scheme 3

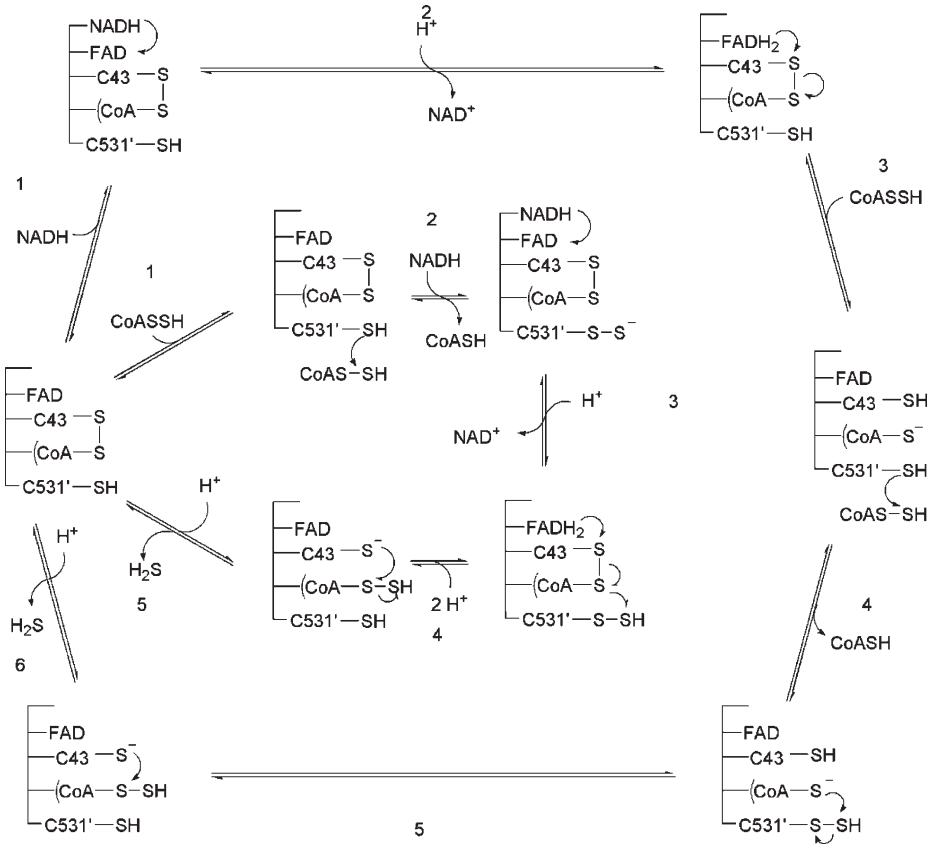

significantly from findings with the *B. anthracis* enzyme, where only 4% activity was observed without the rhodanese domain cysteine (*32*). However, the conditions under which this activity was determined (such as substrate concentrations) were not defined nor were kinetic parameters presented. The kinetics data from the C531S mutant with DTNB does support the idea that this alternative pathway for DTNB reduction is more difficult than the pathway used when this residue is present, as the K_m increases and k_{cat} decreases significantly with this mutation.

The narrowness of the observed substrate channel could explain the differences observed between DTNB reductase and coenzyme A persulfide reductase activity. As a smaller substrate, it seems that DTNB should be able to interact directly with the bound coenzyme A molecule without first interacting with the rhodanese cysteine or even reach the active site directly without the aid of the bound CoA. The coenzyme A or glutathione persulfide substrates are much larger and therefore likely too bulky to follow this already unfavorable alternative pathway and thus show no detectable activity without the presence of C531; the lack of activity with the TNB-persulfide substrate, however, suggests that a less obvious explanation is needed to fully explain the lack of persulfide reductase activity observed with the C531S mutant. Scheme 2 shows the two proposed mechanisms for DTNB reduction for the C531S mutant. DTNB reduction can occur via the initial reaction of DTNB with the C43 residue (upper mechanism) or the CoA thiol (lower mechanism), with release of a second TNB resulting in reformation of oxidized enzyme in the C43-CoA mixed-disulfide form.

Anaerobic Titrations. The initial blue shift observed with the first equivalent of reducing agent indicates a change in the environment of the flavin, while no reduction of the flavin itself occurs. The disappearance of this blue shift (and the first phase of reduction) with the substitution of the C43 residue implies that the first equivalent of reducing agent during titration of wild-type enzyme is modifying the oxidation state of this residue. For this to occur, C43 must exist in an oxidized state, such as a disulfide bond or a sulfenic acid that would then be reduced to a Cys−SH. Examination of the crystal structures indicates the oxidized state of the enzyme to be a coenzyme A−cysteine mixed disulfide bond (Figure 5C). Formation of the reduced cysteine would be required to prepare the active site to reduce the substrate. This mixed disulfide is observed in the *B. anthracis* CoADR-RHD enzyme, as well as in the *S. aureus* and *B. anthracis* CoADR enzymes, which are homologous in the flavoprotein domain only (*15*, *32*, *53*).

Even with this knowledge, the lack of blue shift for the reduction of the C531S mutant with TCEP is still puzzling, as the disulfide bond between C43 and the coenzyme A molecule exists in this structure. This result may have implications for the mechanism by which TCEP reduces the C43-Coenzyme A disulfide on the wild-type enzyme. If the TCEP molecule must first interact with the C531 residue, as appears to be required for the persulfide substrates, no reduction of a C43 mixed disulfide would be observed in the mutant (Schemes 1 and 3).

The anaerobic titrations also provide additional information on the nature of the reductive half-reaction. The inability of NADH to reduce the second flavin indicates subunit asymmetry such that reduction of the FAD on one subunit affects the reduction potential of the FAD on the opposite subunit. Such changes have been observed with both the thermo and mesophilic CoADRs and are therefore not unexpected (*16*, *19*). On the basis of the reduction potential of NADH → NAD^+ (−320 mV) and Ti(III) → Ti(II) (−369 mV), the reduction potential of the first FAD on the wild-type enzyme is higher than −320 mV, and with

its reduction, the second FAD molecule's reduction potential shifts to between −320 and −369 mV. Presteady-state stopped-flow kinetics indicates that the reduction of the flavin itself (to the EH_4 form) occurs much too slowly to be important for catalysis (data not shown). Despite this, the complexity of the reductive half-reaction suggests that the half-site reactivity may still be relevant to the overall mechanism. The kinetics and primary isotope effects of the initial reduction of the flavin (formation of EH_2) with NADH suggests that the reduction occurs at two distinct rates, consistent with half-site inequivalence affecting the mechanism of the $E \rightarrow EH_2$ reaction, an area in which research is ongoing.

While the wild-type enzyme completes its half-reduction of the FAD during the addition of ~1 equiv of NADH (following the completion of the first phase of the reaction), the C43S enzyme requires an excess of NADH to even bring about half-reduction of the FAD, as can be seen by the consistent increase at 340 nm during the addition of NADH. As seen in Figure 2B, addition of 5 equiv of NADH is not enough to cause even half reduction of the FAD. This result suggests that the C43S mutant may have a larger equilibrium constant for formation of the $E/E(FADH_2)$ species. The development of a broad long wavelength absorbance during the first and second phases of the titration is consistent with binding of reduced pyridine nucleotide (*19*, *54*). It seems likely that this absorbance spectrum represents an E·NADH form of the enzyme; comparison of this absorbance spectrum to that of the E·NADH form of the NADH peroxidase (*55*) and an H10A mutant of Npx (*56*) that predominate during turnover is also consistent with this assignment.

The behavior of the Npsr C43S enzyme is very different from that of the C43S mutant of the *S. aureus* CoADR, in which the subunit asymmetry is lost, and full reduction of the FAD occurs during the addition of 1 equiv of NADH (*16*). In the case of Npsr, the subunit asymmetry is maintained, and the reduction of the half equiv of FAD appears to be more difficult than with the wild-type Npsr, since it occurs over the addition of 5−10 equiv of NADH rather than over just 1 equiv of NADH (Figures 2B and 3B).

Proposed Mechanism. On the basis of the aforementioned structural and kinetic information, we propose a new model for the reduction of coenzyme A persulfide that combines the results from the crystal structures as well as kinetic and thermodynamic titrations and knowledge presented from the *B. anthracis* structure (*32*) (Scheme 3). Initially, reduction of the active site cysteine (C43)−coenzyme A bond occurs via NADH thereby priming the active site for reduction of an incoming substrate. Next, a coenzyme A persulfide substrate (or other persulfide), attracted by the positively changed residues surrounding the entrance to the substrate channel, would be positioned to react with the rhodanese domain cysteine (C531) on the alternate subunit of the dimer and transfer sulfur to the enzyme. The bound coenzyme A cofactor, now held tightly by noncovalent interactions, would swing out of the pocket to attack the distal sulfur on the rhodanese cysteine persulfide and then swing back into the active site, where reduction of the CoA−S−SH and release of H_2S would occur, with the coenzyme A−C43 S−S bond restored for the next round of reduction. This model would allow the regenerated coenzyme A product left from the persulfide substrate to leave either after reaction with the C531 residue or following the reaction with the bound coenzyme A. An alternate mechanism (inner circle of Scheme 3), which could operate concurrently with the outer mechanism, can be written in which C531 attacks a persulfide substrate while the active site remains in the oxidized form.

Implications for Sulfur Respiration in Shewanella loihica PV-4. Studies in *S. oneidensis* MR-1 have confirmed that the PsrABC complex is responsible for sulfur reduction in that organism (*12*, *14*, *57*). While the direct electron donor to the PsrABC complex is not known, both H_2 and lactate are able to serve as electron donors to sulfur *in vivo*, and membrane fractions from *Wolinella* are able to use hydrogen in the reduction of sulfur. It seems likely that the presence of Npsr in *S. loihica* PV-4 and its homologue in *S. frigidamarina* provide those organisms with a mechanism for directly reducing sulfur with NADH, immediately regenerating NAD^+ for metabolic purposes.

CONCLUSIONS

The goal of this study was to investigate the mechanism of sulfur reduction in the enzyme NADH-dependent persulfide reductase (Npsr) from *Shewanella loihica* PV-4. The data presented indicates coenzyme A persulfide and other persulfides to be the *in vivo* substrates of this enzyme. The active site cysteine (C43) and the cysteine within the rhodanese domain (C531) are both essential for the mechanism of the enzyme, as demonstrated by serine mutations at these residues. The crystal structure shows a bound chloride ion adjacent to the C531 residue. This location appears to be where the persulfide sulfur of the thiol-persulfide substrate binds prior to interaction with the rhodanese domain cysteine. This suggests a mechanistic explanation for the importance of the C531 residue. Reductive titrations indicate a change in oxidation state in the environment of the FAD isoalloxazine ring, and titration with TCEP shows that the first phase of this reduction involves breakage of a sulfur−sulfur bond. The crystal structure shows that the oxidized form of the enzyme is a mixed disulfide between C43 and coenzyme A, and it is this disulfide bond which is reduced during the first phase of the reduction. Interestingly, lack of the both the C43 and C531 residues does not release the coenzyme A molecule. While our kinetic data is consistent with the mechanism presented by Wallen et al. (*32*), the lack of the cysteine−coenzyme A bond in the mutant enzyme does not release the pantetheine arm as observed with synchrotron radiation induced reduction of the wild-type enzyme.

REFERENCES

1. Nealson, K. (1997) Sediment bacteria: Who's there, what are they doing, and what's new? *Annu. Rev. Earth Planet. Sci. 25*, 403–434.
2. Nealson, K. H., Belz, A., and McKee, B. (2002) Breathing metals as a way of life: geobiology in action. *Antonie Van Leeuwenhoek 81*, 215–222.
3. Fredrickson, J. K., and Balkwill, D. L. (2006) Geomicrobial processes and biodiversity in the deep terrestrial subsurface. *Geomicrobiol. J. 23*, 345–356.
4. Castresana, J., and Moreira, D. (1999) Respiratory chains in the last common ancestor of living organisms. *J. Mol. Evol. 49*, 453–460.
5. Vargas, M., Kashefi, K., Blunt-Harris, E. L., and Lovley, D. R. (1998) Microbiological evidence for Fe(III) reduction on early Earth. *Nature 395*, 65–67.
6. Hedderich, R., Klimmek, O., Kroger, A., Dirmeier, R., Keller, M., and Stetter, K. O. (1998) Anaerobic respiration with elemental sulfur and with disulfides. *FEMS Microbiol. Rev. 22*, 353–381.
7. Hille, R. (2002) Molybdenum and tungsten in biology. *Trends Biochem. Sci. 27*, 360–367.
8. Bordo, D., and Bork, P. (2002) The rhodanese/Cdc25 phosphatase superfamily. Sequence-structure-function relations. *EMBO Rep. 3*, 741–746.
9. Lin, Y. J., Dancea, F., Lohr, F., Klimmek, O., Pfeiffer-Marek, S., Nilges, M., Wienk, H., Kroger, A., and Ruterjans, H. (2004) Solution

structure of the 30 kDa polysulfide-sulfur transferase homodimer from *Wolinella succinogenes*. *Biochemistry 43*, 1418–1424.
10. Klimmek, O., Stein, T., Pisa, R., Simon, J., and Kroger, A. (1999) The single cysteine residue of the Sud protein is required for its function as a polysulfide-sulfur transferase in *Wolinella succinogenes*. *Eur. J. Biochem. 263*, 79–84.
11. Klimmek, O., Kreis, V., Klein, C., Simon, J., Wittershagen, A., and Kroger, A. (1998) The function of the periplasmic Sud protein in polysulfide respiration of *Wolinella succinogenes*. *Eur. J. Biochem. 253*, 263–269.
12. Burns, J. L., and DiChristina, T. J. (2009) Anaerobic respiration of elemental sulfur and thiosulfate by *Shewanella oneidensis* MR-1 requires psrA, a homolog of the phsA gene of Salmonella enterica serovar typhimurium LT2. *Appl. Environ. Microbiol. 75*, 5209–5217.
13. Gralnick, J. A., Vali, H., Lies, D. P., and Newman, D. K. (2006) Extracellular respiration of dimethyl sulfoxide by *Shewanella oneidensis* strain MR-1. *Proc. Natl. Acad. Sci. U.S.A. 103*, 4669–4674.
14. Moser, D. P., and Nealson, K. H. (1996) Growth of the facultative anaerobe *Shewanella putrefaciens* by elemental sulfur reduction. *Appl. Environ. Microbiol. 62*, 2100–2105.
15. Mallett, T. C., Wallen, J. R., Karplus, P. A., Sakai, H., Tsukihara, T., and Claiborne, A. (2006) Structure of coenzyme A-disulfide reductase from *Staphylococcus aureus* at 1.54 A resolution. *Biochemistry 45*, 11278–11289.
16. Luba, J., Charrier, V., and Claiborne, A. (1999) Coenzyme A-disulfide reductase from *Staphylococcus aureus*: evidence for asymmetric behavior on interaction with pyridine nucleotides. *Biochemistry 38*, 2725–2737.
17. delCardayre, S. B., Stock, K. P., Newton, G. L., Fahey, R. C., and Davies, J. E. (1998) Coenzyme A disulfide reductase, the primary low molecular weight disulfide reductase from *Staphylococcus aureus*. Purification and characterization of the native enzyme. *J. Biol. Chem. 273*, 5744–5751.
18. Schut, G. J., Bridger, S. L., and Adams, M. W. (2007) Insights into the metabolism of elemental sulfur by the hyperthermophilic archaeon *Pyrococcus furiosus*: Characterization of a coenzyme A- dependent NAD(P)H sulfur oxidoreductase. *J. Bacteriol. 189*, 4431–4441.
19. Harris, D. R., Ward, D. E., Feasel, J. M., Lancaster, K. M., Murphy, R. D., Mallet, T. C., and Crane, E. J., 3rd. (2005) Discovery and characterization of a Coenzyme A disulfide reductase from *Pyrococcus horikoshii*. Implications for this disulfide metabolism of anaerobic hyperthermophiles. *FEBS J. 272*, 1189–1200.
20. Claiborne, A., Yeh, J. I., Mallett, T. C., Luba, J., Crane, E. J., 3rd, Charrier, V., and Parsonage, D. (1999) Protein-sulfenic acids: diverse roles for an unlikely player in enzyme catalysis and redox regulation. *Biochemistry 38*, 15407–15416.
21. Li, H. W., Yang, F., Kang, X., Xia, B., and Jin, C. W. (2008) Solution structures and backbone dynamics of *Escherichia coli* rhodanese PspE in its sulfur-free and persulfide-intermediate forms: Implications for the catalytic mechanism of rhodanese. *Biochemistry 47*, 4377–4385.
22. Cipollone, R., Ascenzi, P., and Visca, P. (2007) Common themes and variations in the rhodanese superfamily. *IUBMB Life 59*, 51–59.
23. Mueller, E. G. (2006) Trafficking in persulfides: delivering sulfur in biosynthetic pathways. *Nat. Chem. Biol. 2*, 185–194.
24. Mintel, R., and Westley, J. (1966) The rhodanese reaction. Mechanism of sulfur-sulfur bond cleavage. *J. Biol. Chem. 241*, 3381–3385.
25. Mintel, R., and Westley, J. (1966) The rhodanese reaction. Mechanism of thiosulfate binding. *J. Biol. Chem. 241*, 3386–3389.
26. Green, J. R., and Westley, J. (1961) Mechanism of rhodanese action: polarographic studies. *J. Biol. Chem. 236*, 3047–3050.
27. Westley, J., and Green, J. R. (1959) Crystalline beef kidney rhodanese. *J. Biol. Chem. 234*, 2325–2326.
28. Cipollone, R., Ascenzi, P., Frangipani, E., Visca, P. (2005) Cyanide detoxification by recombinant bacterial rhodanese, *Chemosphere*.
29. Cipollone, R., Bigotti, M. G., Frangipani, E., Ascenzi, P., and Visca, P. (2004) Characterization of a rhodanese from the cyanogenic bacterium. *Pseudomonas aeruginosa, Biochem. Biophys. Res. Commun. 325*, 85–90.
30. Wolfe, M. D., Ahmed, F., Lacourciere, G. M., Lauhon, C. T., Stadtman, T. C., and Larson, T. J. (2004) Functional diversity of the rhodanese homology domain: the *Escherichia coli* ybbB gene encodes a selenophosphate-dependent tRNA 2-selenouridine synthase. *J. Biol. Chem. 279*, 1801–1809.
31. Lukose, V., Lopez, K., Crane, E. J., 3rd. (2008) Discovery and characterization of an NADH-dependent polysulfide reductase flavoprotein (Npsr) from Shewanella loihica PV-4: Implications for dissimilatory sulfur reduction in the genus Shewanella, in Flavins and Flavoproteins (Medina, M., Ed.) pp 375−380, Prensas Universitarias de Zaragoza; Zaragoza, Spain.
32. Wallen, J. R., Mallett, T. C., Boles, W., Parsonage, D., Furdui, C. M., Karplus, P. A., and Claiborne, A. (2009) Crystal structure and catalytic properties of *Bacillus anthracis* CoADR-RHD: implications for flavin-linked sulfur trafficking. *Biochemistry 48*, 9650–9667.
33. Fauque, G., Klimmek, O., Kroger, A. (1994) Sulfur Reductases from spirilloid mesophilic sulfur-reducing eubacteria, in Methods in Enzymology (Peck, H. D. L. J., Ed.) pp 367−383, Academic Press, San Diego, CA.
34. Brooks, S. P. (1992) A simple computer program with statistical tests for the analysis of enzyme kinetics. *Biotechniques 13*, 906–911.
35. Otwinowski, Z., and Minor, W. (1997) Processing of X-ray diffraction data collected in oscillation mode. *Methods Enzymol. 276*, 307–326.
36. McCoy, A. J., Grosse-Kunstleve, R. W., Adams, P. d., Winn, M. D., Storoni, L. C., and Read, R. J. (2007) Phaser crystallographic software. *J. Appl. Crystallogr. 40*, 658–674.
37. Emsley, P., and Cowtan, K. (2004) Coot: Model-building tools for moleclar graphics. *Acta Crystallogr., Sect. D 60*, 2126–2132.
38. Murshudov, G. N., Vagin, A. A., and Dodson, E. J. (1997) Refinement of macromolecular structures by the maximum-likelihood method. *Acta Crystallogr. D53*, 240–255.
39. Collaborative Computational Project, N (1994) The CCP4 suite programs for protein crystallography. *Acta Crystallogr. D50*, 760–763.
40. Laskowski, R. A., MacArthur, M. W., Moss, D. S., and Thornton, J. M. (1993) PROCHECK: a program to check the stereochemical quality of protein structures. *J. Appl. Crystallogr. 26*, 283–291.
41. Kamyshny, A., Jr. (2009) Solubility of cyclooctasulfur in pure water and sea water at different temperatures. *Geochim. Cosmochim. Acta 73*, 6022–6028.
42. Falk, M. C., Johnson, P. G., and McCormick, D. B. (1976) Synthetic flavinyl peptides related to the active site of mitochondrial monoamine oxidase. I. Chemical and spectral properties. *Biochemistry 15*, 639–645.
43. Penzer, G. R., and Radda, G. K. (1967) Chemistry and Biological Function of Isoalloxazines (Flavines). *Q. Rev. Chem. Soc. 21*, 43–65.
44. Penzer, G. R., and Radda, G. K. (1967) Flavins in a Solid Matrix. *Nature 213*, 251–253.
45. Burns, J. A., Butler, J. C., Moran, J., and Whitesides, G. M. (1991) Selective reduction of disulfides by tris(2-carboxyethyl)phosphine. *J. Org. Chem. 56*, 2648–2650.
46. Westley, J., and Nakamoto, T. (1962) Mechanism of rhodanese action: isotopic tracer studies. *J. Biol. Chem. 237*, 547–549.
47. Engst, S., and Miller, S. (1999) Alternative Routes for Entry of HgX_2 into the Active Site of Mercuric Ion Reductase Depend on the Nature of the X Ligands. *Biochemistry 38*, 3519–3529.
48. Schiering, N., Kabsch, W., Moore, M. J., Distefano, M. D., Walsh, C. T., and Pai, E. F. (1991) Structure of the detoxification catalyst mercuric ion reductase from *Bacillus sp*. strain RC607. *Nature 352*, 168–172.
49. Cheng, Q., Sandalova, T., Lindqvist, Y., and Arner, E. S. (2009) Crystal structure and catalysis of the selenoprotein thioredoxin reductase 1. *J. Biol. Chem. 284*, 3998–4008.
50. Williamson, G., Engel, P. C., Mizzer, J. P., Thorpe, C., and Massey, V. (1982) Evidence that the greening ligand in native butyryl-CoA dehydrogenase is a CoA persulfide. *J. Biol. Chem. 257*, 4314–4320.
51. Shaw, L., and Engel, P. C. (1987) CoA-persulphide: a possible in vivo inhibitor of mammalian short-chain acyl-CoA dehydrogenase. *Biochim. Biophys. Acta 919*, 171–174.
52. delCardayre, S. B., and Davies, J. E. (1998) *Staphylococcus aureus* coenzyme A disulfide reductase, a new subfamily of pyridine nucleotide-disulfide oxidoreductase. sequence, expression, and analysis of cdr. *J. Biol. Chem. 273*, 5752–5757.
53. Wallen, J. R., Paige, C., Mallett, T. C., Karplus, P. A., and Claiborne, A. (2008) Pyridine nucleotide complexes with *Bacillus anthracis* Coenzyme A-disulfide reductase: a structural analysis of dual NAD(P)H specificity. *Biochemistry 47*, 5182–5193.
54. Poole, L. B., and Claiborne, A. (1986) Interactions of pyridine nucleotides with redox forms of the flavin- containing NADH peroxidase from *Streptococcus faecalis*. *J. Biol. Chem. 261*, 14525–14533.
55. Crane, E. J., 3rd, Parsonage, D., Poole, L. B., and Claiborne, A. (1995) Analysis of the kinetic mechanism of enterococcal NADH peroxidase reveals catalytic roles for NADH complexes with both oxidized and two- electron-reduced enzyme forms. *Biochemistry 34*, 14114–14124.
56. Crane, E. J., 3rd, Parsonage, D., and Claiborne, A. (1996) The active-site histidine-10 of enterococcal NADH peroxidase is not essential for catalytic activity. *Biochemistry 35*, 2380–2387.
57. Moser, D. P. (1996) Elemental sulfur reduction in *Shewanella putrafaciens*, Ph.D. Dissertation, p 207, University of Wisconsin-Milwaukee, Milwaukee, WI.